Two Photon Excitable Iridium Complex containing Dipyrazolyltriazine as Cellular Imaging Dyes

Poonnapa Zheng,[a] Pawittra Chaibuth,[c] Wai-Sum Lo,[a] Weiweij Jin,[d] Xinyang Sun,[a] Sureemas Meksawangwong,[c] Wikorn Punyain,[c] Miroslav Gál,[e] Yanjuan Gu,[a]] Wesley Ting Kwok Chan,[a] Filip Kielar*,[c] Ga-Lai Law*[a][b]

Abstract: In this work, the synthesis, stability studies and photophysical properties of a bis-cyclometalated iridium(III) complex with a push-pull ancillary ligand are presented. The complex was found to localize in mitochondria and could be excited by a two-photon excitation process under a confocal laser scanning microscope.

Introduction

Luminescent cyclometalated Ir(III) complexes have been receiving a huge amount of attention for their luminescent properties and thermal stability, making them interesting compounds for use in applications such as organic light emitting diodes (OLEDs), photoredox catalysis, and biological imaging.[1] Among other properties, the Ir(III) ion exhibits a large spin-orbit coupling effect[2], which facilities efficient intersystem crossing, leading to the population of the chromophore's triplet state and results in luminescence with long lifetimes, as well as giving a large Stokes' shift. Ir(III) complexes can be found in two major forms[1a]: homoleptic complexes consisting of three identical ligands most usually cyclometalated with the Ir(III) center; whereas when one of the cyclometalated ligands is replaced by another ligand (e.g. a diamine N^N ligand such as 2,2'-bypiridine), heteroleptic complexes are obtained. One of the major benefits of using Ir(III) complexes as luminescent agents is the freedom for color tuning by inserting various types of ancillary ligands.[3] This is facilitated by the fact that the HOMO and LUMO orbitals of such complexes reside on different portions of the molecule, meaning that their energies can be tuned independently by structural modification. For biscyclometalated complexes the HOMO usually resides on the metal and the cyclometalating N^C ligands while the LUMO is usually located on the ancillary N^N ligand.[1b] The triplet state of the ancillary ligand would be populated either by spin-orbit effect of the Ir(III) or by the redistribution of the excitation energy of the cyclometalated ligands within the Ir(III) complex. It has been found that the emission from the triplet excited state through a metal to ligand charge transfer (MLCT) state or a mixing of MLCT and ligand-centered (LC) states are key to successful color tunability.[4]

Many types of ligands are used to form iridium complexes. The most common ligands used include 2-phenylpyridine (ppy) as the cyclometalating C^N ligand and derivatives of 2,2'-bypiridine and 1,10-phenanthroline as the ancillary N^N ligands. Synthesis pathways of iridium complex can be separated into 2 main steps. The first step is the Nonoyama reaction or the formation of chloride-bridged dinuclear iridium (III) dimer,[1a,5] the unique structure of the dimer contains four cyclometalating ligands and two chloride bridging ligands. The second step is the splitting of the chloride-bridge, which leads to the complexation reaction with the interested ligands. The Ir–C bond formed between iridium metal and ppy ligands are considered strong therefore iridium complexes with ppy as the cyclometalated ligand usually have exceptionally good thermal stability.[1a]

Given the fact that color tuning of the emission of cyclometalated iridium complexes can be achieved by changing the ancillary N^N ligands, it is still of interest to prepare new iridium complexes containing new ligand structures. We therefore set out to prepare biscyclometalated iridium complexes using ligands **L1-L3**. The N^N ligands **L1**-**L3** of interest in this work possess an intra-ligand charge transfer (ILCT) band due to their push-pull structure:[6] the diethylamino group acts as an electron donor and the dipyrazolyltriazine acts as an electron acceptor, bridged by a phenyl ring. Their CT character gives them intrinsically high extinction coefficients and they are thus useful for designing biological probes, when the parameter brightness (ε x Φ) is vital. The D-π-A design of these ligand structures is also advantageous towards imparting the complex with multi-photon excitation properties,[7] which prevents damages to living cells caused by high energy UV photons and has higher penetration through tissues.[8] Fluorescent biological entities are also rarely excited by multi-photon excitation, hence eliminating interferences in imaging experiments.

In this work, we discuss the synthesis, photophysical properties and cellular imaging properties of a novel iridium complex and assess its potential in becoming optical probes in bio-imaging.

Results and Discussion

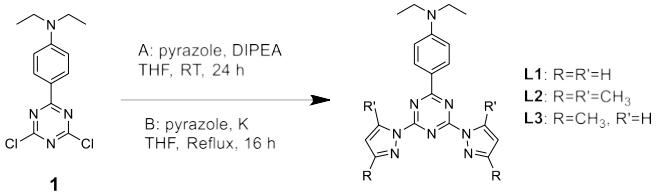

1

Scheme 1. Synthetic scheme of L1-L3.

[a] Department of Applied Biology and Chemical Technology, The Hong Kong Polytechnic University, Hung Hom, Hong Kong SAR, China
[b] The Hong Kong Polytechnic University, Shenzhen Research Institute, Shenzhen, China. E-mail: ga-lai.law@polyu.edu.hk
[c] Department of Chemistry, Naresuan University, Phitsanulok, 65000, Thailand Email: filipkielar@nu.ac.th
[d] College of Chemistry & Chemical Engineering, Xinjiang University, Urumqi, 830046, China
[e] Department of Inorganic Technology, Slovak University of Technology, Bratislava, 812 37, Slovakia
Supporting information for this article is given via a link at the end of the document.

Ligands **L1**-**L3** were synthesized by incorporating the pyrazoles into the diethylanilinyl-triazine core (**1**). It is because the substitution of the chlorides of cyanuric chloride becomes increasingly difficult upon each successive substitution, and it was found out that the diethylaniline moiety could not be added as the third substituent even if the n-butyllithium synthetic route was applied; therefore, the pyrazoles, with a higher basicity and stability at higher temperature, were added last. The purification, however, was not straightforward. Despite separating the desired product from un-substituted impurities by column chromatography, the product was often eluted with a non-polar impurity which appeared lilac under 365 nm excitation of a handheld UV lamp on a TLC plate. Reversed phase semi-preparative HPLC was used to ensure purity of the ligands.

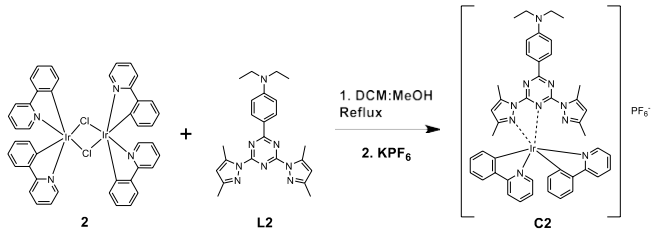

Scheme 2. Synthetic scheme of **C2**.

The Ir(III) dimer **2** was synthesized successfully according to literature procedure and was used to react with ligands **L1**-**L3** in order to form the desired biscyclometalated iridium complexes. This reaction was carried out in two different solvent systems. Initially, the commonly used mixture of dichloromethane and methanol was used. Unfortunately, only complex **C2** could be obtained in a moderate yield. Reaction mixtures made using **L1** and **L3**, did not even contain the expected m/z peaks of **C1** and **C3**. However, m/z peaks of alternate products where one of the pyrazole rings seems to have been replaced by methanol have been observed (Figure 1).

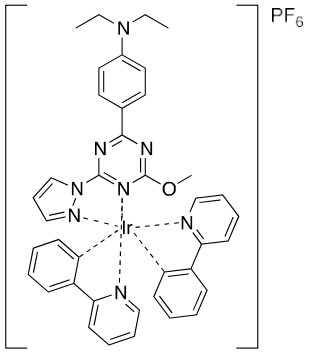

Figure 1. Structure of suspected product formed during the complexation of ligand **L1**.

This was further corroborated by the ^{1}H NMR spectrum of the product isolated from the reaction employing **L1**, which contains a signal at 3.586 ppm expected to be from the methoxy group. Furthermore, it was observed that when ligand **L1** was allowed to rest at the complexation conditions, a m/z peak suggesting the substitution of both pyrazole rings by methoxy groups could be observed in mass spectra whereas no decomposition was observed for ligand **L2** under the same conditions. Thus, we presume the presence of the methyl groups in **L2** exerts a protective effect of electronic and steric natures. It is also apparent that the pyrazole ring's participation in coordination restricts displacement by methanol as in the complex based on **L1**, only one of the pyrazoles was substituted (Figure 1). These observations led to trials of alternate reaction conditions, where acetonitrile was used instead of methanol in the reaction solvent. While the mass spectra of the crudes of **C1** and **C3** displayed the m/z peaks corresponding to their respective molecular ions along with other peaks, none of the tried purification methods gave a clean TLC trace, ^{1}H or ^{13}C spectra, or mass spectra. In fact, injecting the crudes into reversed-phase semi-preparative HPLC with ACN, methanol, or acetone as eluent resulted in the generation of more species. It should also be noted that complex **C2** was isolated in much lower yield when these reaction conditions were used (*vide infra*).

As the three complex structures differ only in the number of methyl groups on the pyrazole rings, it is suspected that the electron donating property of methyl groups is instrumental in stabilizing the complex by increasing the donor strength of the nitrogen atom and therefore result in stronger bonding interactions; whereas one or no methyl groups is not enough. In latter cases, the iridium center will become susceptible to coordination of solvent molecules, such as the more nucleophilic acetonitrile molecule. The absorbances of the **C2** in different solvents were monitored by UV-Vis spectroscopy to investigate its solution state stability over time, under the assumption that any instability would occur more rapidly in **C1** and **C3** (*vide infra*). Eventually, out of the three proposed complexes, only **C2** was successfully synthesized, and it was characterized by ^{1}H, ^{13}C, mass spectroscopy and X-ray diffraction (Figure 2). (CCDC-1561475)

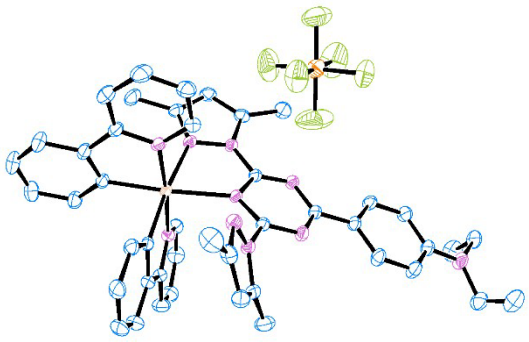

Figure 2. X-ray crystal structure of complex **C2** (H atoms and solvent molecule hidden for clarity).

Based on the NMR spectra, the solution state structure of complex **C2** lacks symmetry as indicated by the solid state structure obtained from X-ray diffraction, which is evident from the presence of separate signals for the two 2-phenylpyridine ligands. Furthermore, the broadening of the signal observed at 9.429 ppm hints at the possibility of dynamic processes within the structure. Therefore, variable temperature ^{1}H-NMR experiment was performed with complex **C2** between 298 K and 193 K (Figure S17). Further broadening of this signal as well as of several other aromatic signals from the 2-phenylpyridine ligand is observed at 273 K and 253 K followed by appearance of sharper signals at 233 K. These observations indicate the transition of the dynamic process from a relatively fast regime on NMR time scale at 298 K to a slow regime at 233 K. The process could indicate fluxionality with respect to the unbound pyrazole donor.

Photophysical Properties

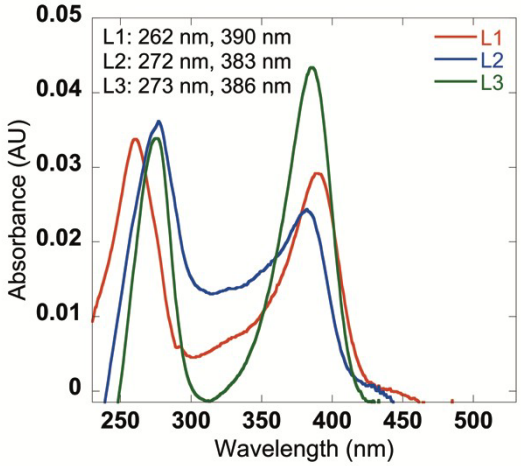

Figure 3. UV-Vis absorption spectra of ligands **L1**-**L3** in DCM.

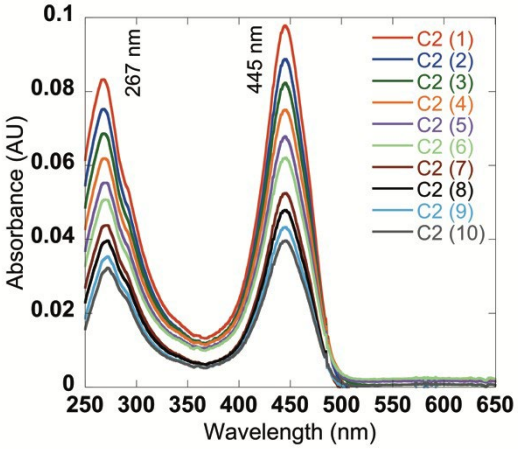

Figure 4. UV-Vis absorption spectrum of **C2** in DCM upon serial dilution.

Figure 3 shows the absorption spectra of ligands **L1**-**L3** in DCM, there are two major peaks: the higher energy band is assigned to the π–π^* transition of the dipyrazolyltriazine part and the lower energy band with the absorption maximum at around 390 nm is assigned to the n-π^* transitions of the diethylaniline moiety. The shifts in the absorption maxima amongst the ligands are expected due to the change in electronic environment brought about by the number of methyl substituents. The molar extinction coefficients are summarized in Table 1. The absorption spectrum of **C2** is presented in Figure 4. The absorption maximum of the CT transition is significantly shifted to 445 nm, a result of coordination with the electropositive Ir(III) center which extends and stabilizes the electronic conjugation system of the ancillary ligand; the molar extinction coefficient was also more than tripled compared to the free ligand. The shoulder peak at around 285 nm corresponds to the absorption of the cyclometalating phenylpyridine ligand. It should be noted that the presence of the intense absorption peak in the visible region for complex **C2** is interesting as one of the shortcomings of luminescent iridium complexes is their weak absorption of light in this part of the spectrum.

Table 1. Summary of molar extinction coefficients in DCM.

Compound	L1	L2	L3	C2
Absorbance (nm)	390	383	386	445
ε (x 10^6 mol^{-1}cm^{-1}L)	1.68	1.44	3.85	4.86

As mentioned previously, the solution state stability of the complexes is affected by the number of methyl substituents on the pyrazole rings and can be monitored using UV-Vis absorption spectroscopy. As seen in Figure 4, dilution of **C2** did not result in any change in the UV-Vis absorption spectral profile, suggesting the complex structure was retained with increasing concentration of solvent molecules. Another DCM solution of **C2** was left idle for 3 hours at room temperature and its absorption was monitored at regular time intervals (Figure 5). The variation over time was little, once again demonstrating the solution state stability of **C2**.

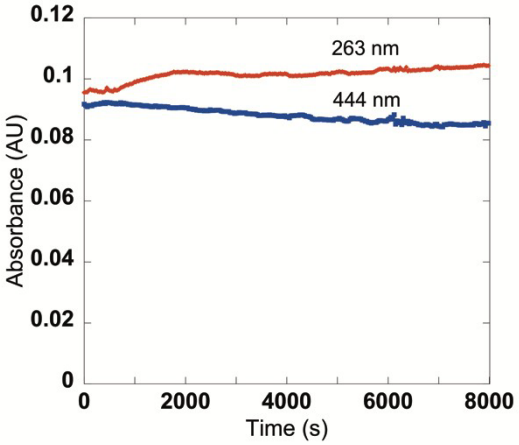

Figure 5. Various absorbance intensities of **C2** in DCM over time.

When the solvent was changed to methanol, however, a fluctuating yet seemingly regular pattern is observed. In Figure 6, the drop of the 263 nm absorption is accompanied by the rise of

the 436 nm absorption, although the extent of variation is not the same – suggesting that the rise and drop result from the same structural change. This oscillating behavior suggests the possibility of existence of competing pathways for the rather sluggish displacement of the ancillary ligand with methanol that form and consume a common intermediate. Such pathways could involve an alternative order of displacement of the triazine and pyrazole donors.

In Figure 7, the UV-Vis absorption was monitored in ACN. The peak at 434 nm was observed when **C2** was freshly dissolved in ACN and was assigned as the ILCT absorption of the ancillary ligand. After approximately 16 hours, a steady drop was observed for the peak at 434 nm which was accompanied by the simultaneous rise of the absorption at 385 nm, corresponding to the absorption of the free, uncoordinated ancillary ligand displaced by ACN molecules (Figure 7 and 8).

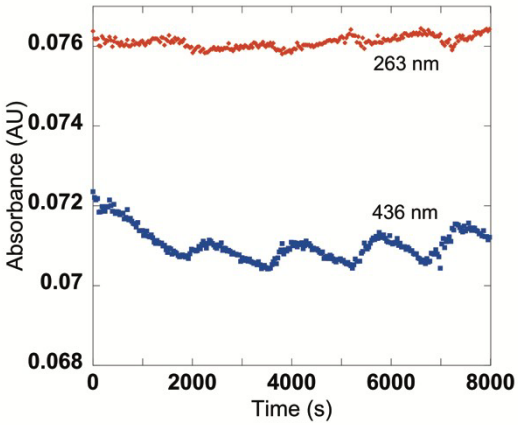

Figure 6. Various absorbance intensities of **C2** in MeOH over time.

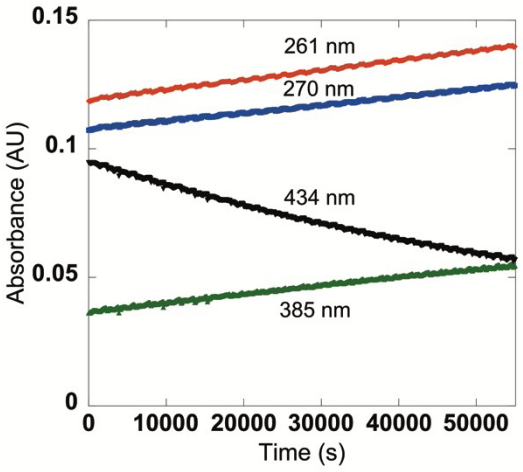

Figure 7. Various absorbance intensities of **C2** in ACN overnight.

Compared to in DCM and MeOH, **C2** is clearly unstable in ACN due to solvent coordination.[4e] This result also explains the extremely low yield (6.1%) of synthesizing **C2** in a DCM:ACN solvent mixture, due to dominant competition with the ancillary ligand for coordination to the Ir(III) center. In **C1** and **C3**, with less and no methyl substituents, the coordination strength of the ancillary ligand is weaker, and their syntheses are understandably unsatisfactory.

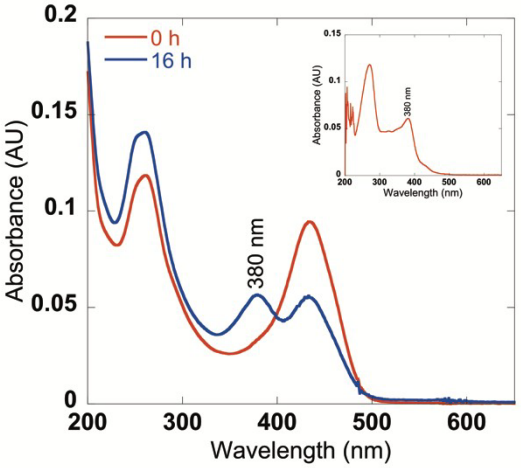

Figure 8. UV-Vis absorption spectra of C2 (left; red: freshly dissolved; blue: after 16 hours) and L2 (right) in ACN.

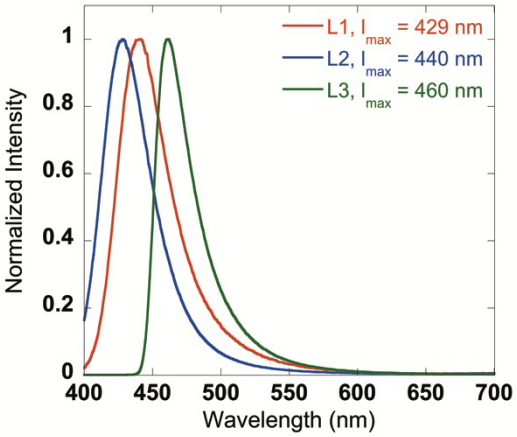

Figure 9. Normalized emission spectra of **L1-L3** in DCM excited at their absorption maxima.

Figure 9 shows the emission spectra of the ligands **L1-L3** in DCM. The electronic effect of the methyl substituents is clearly observed in the different emission peak maxima, with **L2** and **L1** exhibiting blue- and red-shift with respectively from **L3**. The emission and excitation spectra of **C2** is presented in Figure 10. The most intense excitation band is assigned to the ILCT transition of the ancillary ligand and the emission band that mirror-images it is assigned to the fluorescence of the same ligand. The ancillary ligand, upon coordination, has an emission profile remarkably different than the free ligand, with its peak maximum red-shifted from 429 nm to 475 nm.

The secondary, broader emission band with a maximum at *ca.* 600 nm, absent in the emission of **L2**, is assigned as the phosphorescence originating from the MLCT transitions within the complex, facilitated by the spin-orbit coupling effect of the nearby

Ir(III) center. As seen, the phosphorescence intensity is much lower than the ligand fluorescence; this is not surprising as the triplet state of the ancillary ligand was also difficult to induce even in the presence of heavy lanthanide ions. The phosphorescence lifetime was measured in degassed DCM and a biexponential decay was observed, with lifetimes calculated to be 0.36 and 4.21 μs, which might be explained by the dual nature (ILCT, MLCT) of the photophysical properties of this complex.

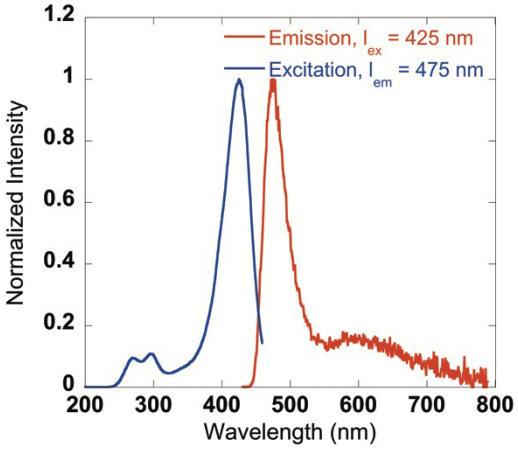

Figure 10. Normalized emission and excitation spectra of **C2** in DCM.

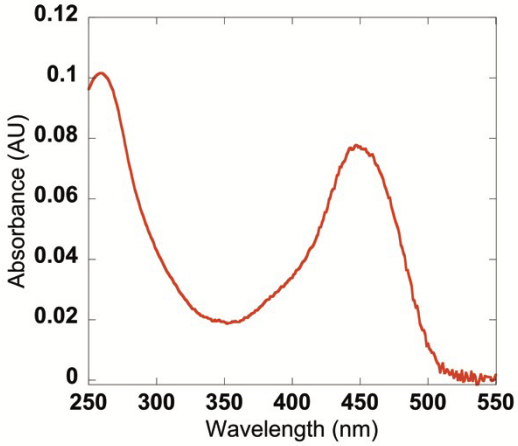

Figure 11. Absorption spectrum of C2 in aqueous solution.

As we intend to utilize the designed complexes as imaging probes, the photophysical properties of **C2** were also studied in an aqueous system (0.1 M HEPES buffer, pH 7.3, 1% DMSO). As the diethylaniline moiety is sensitive to the polarity environment, the difference in solvent polarity between DCM and water is reflected in the spectrophotometric spectra. While the band maxima of the absorption spectra (Figure 11) in aqueous solution remains unchanged compared to DCM, the relative intensities between the π–π* and n–π* transitions are different. On the other hand, there is a marked difference in the emission and excitation spectrum (Figure 12). The phosphorescent MLCT transition is significantly higher than the fluorescence of the ancillary ligand, with the overall emission maximum situated at around 613 nm; this result is a clear indication on how the solvatochromic triazine-based ligand affects the luminescence properties of our Ir(III) complex in solvents with different polarities. The pH sensitivity of **C2** was also investigated using universal TRIS buffer solutions. As seen in Figure S21, the emission profile between pH 3-8 remains the same, only differing in intensity, with the emission intensity is higher when the pH is lower. However, at pH 9 and 10, the emission band is completely different, indicating the existence of a different emitting species.

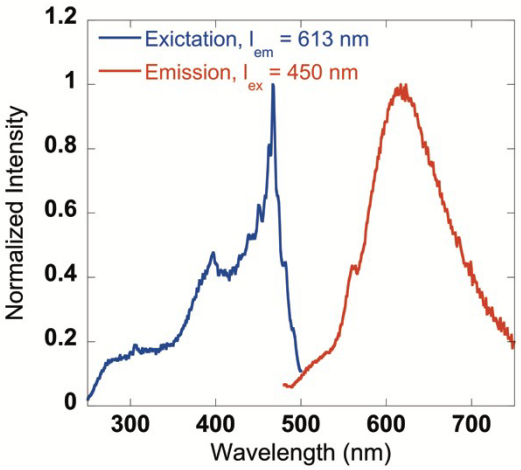

Figure 12. Normalized emission and excitation spectra of **C2** in aqueous solution (~2 μM).

The luminescence decay at 613 nm was measured and fitted as a biexponential decay with lifetimes of 3.84 and 27.6 μs (Figure S21); once again the apparent difference in lifetimes corroborates with the luminescence spectrum that the emitting species in DCM and aqueous solution is different, a property imparted and controlled by the triazine-based ligand.

The intensity of the photoluminescence for C2 is rather low, giving an absolute quantum yield of 0 when measured using an integrating sphere in degassed DCM. Hence we measured the relative quantum yield of C2 against perylene in cyclohexane (Φ = 0.94)[9] and a value of 0.005 was obtained.

Electrochemistry

Cyclic voltammetry (CV) can be used to assess the relative energies of the HOMO and LUMO. The redox behavior of **L2** and **C2** was studied by cyclic voltammetry in 0.1 M $TBAPF_6$ solution in dry acetonitrile using Pt disk electrode as the working electrode (WE). Two quasi-reversible oxidation peaks I and II and one quasi-reversible reduction peak III are visible in Figure 11 for **C2**. The measurements were carried out with freshly prepared solutions as broadening of the features was observed for aged solutions, most likely due to the decomposition discussed above. The peak I at +1.32 V vs RE corresponds to the oxidation of ligands and the second peak II at +1.56 V vs RE to the oxidation of Ir(III) to Ir(IV). This observation is in agreement with HOMO and HOMO-1 calculation. In the case of **L2** the oxidation process is facilitated due to the absence or Ir(III) and peak I is shifted to more

positive potentials (+1.19 V vs RE) and peak II is not observed. The linear dependence of the peak height on the square root of the scan rate confirms that diffusion is the rate determining step during oxidation of metal. However, from the logarithmic dependence of the peak height on the logarithm of scan rate, it is possible to conclude that also some portion of adsorption of reactants at the electrode surface also plays a role in the reaction kinetics. The potential difference between oxidation and reduction of Ir is 60 mV which confirms a one-electron process; however, the height of the respective reduction peak is lower than the height of the oxidation peak of metal. In the case of peak II, the respective reduction peak is almost invisible. The peak that corresponds to the oxidation of Ir(III) is shifted *ca.* 90 mV to the more positive potentials than in the case of the similar compound studied by Ladouceur and Zysman-Colman.[4e] The reduction of compound **C2** at -1.20 V vs RE occurs with respect to LUMO calculation and CV measurements on the triazine ligand. Similar observation was found in the case of $[Ir(ppy)_2bpy](PF_6)$ complex.[4d] The potential difference between oxidation and reduction of **C2** is 2.76 V is ca 100 mV higher than in the case of $[Ir(ppy)_2bpy](PF_6)$ complex.[4d]

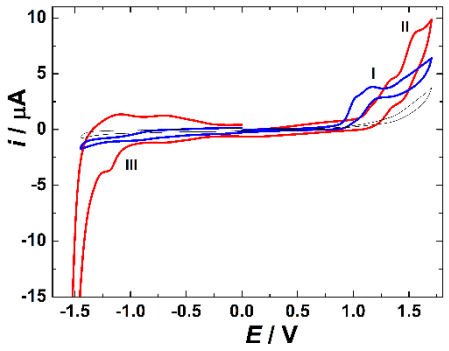

Figure 13. Cyclic voltammograms of baseline (black line), **C2** (red line), and **L2** (blue line) in CH_3CN solution at 25°C.

Theoretical Calculations

Density Functional Theory (DFT) calculations were performed with **C2** in vacuum, acetonitrile, and dichloromethane. The latter two being approximated with the polarizable continuum model. Geometry optimizations and frequency calculations were done at the B3LYP/LANL2DZ level of theory. The results of the calculations are shown in Figures 14-16 and the energies of the orbitals of interest are summarized in Table 2.

Figure 14 depicts the HOMO-1, HOMO, and LUMO orbitals from the calculations. The HOMO orbital (-7.49 eV) shows that the electrons are localized on the iridium atom and the phenyl ring of the cyclometalating ligand phenylpyridine while the electrons of the LUMO orbital (-4.69 eV) are localized along the anilinyl-triazine skeleton of the ancillary ligand.

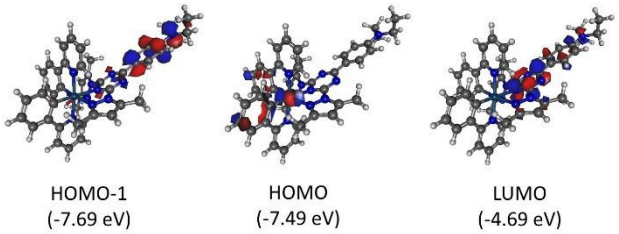

Figure 14. The HOMO and LUMO orbitals of complex **C2** calculated in a vacuum.

These values and orbital distributions are comparable to the values calculated for the prototypical $[Ir(ppy)_2bpy]^+$ (HOMO: -7.82 eV; LUMO: -4.96 eV).[10] This indicates that the HOMO → LUMO transition in **C2** has a metal-to-ligand charge transfer (MLCT) character as the model complex $[Ir(ppy)_2bpy]^+$. However, a feature differentiating **C2** from the model complex is the small energy difference between the HOMO and HOMO-1 orbitals. The HOMO-1 (-7.69 eV) orbital is located on the aniline part of the triazine ligand and is only 0.2 eV lower than the HOMO orbital. The localization is also different as in the $[Ir(ppy)_2bpy]^+$ the HOMO-1 orbital is located on cyclometalating ppy ligands.

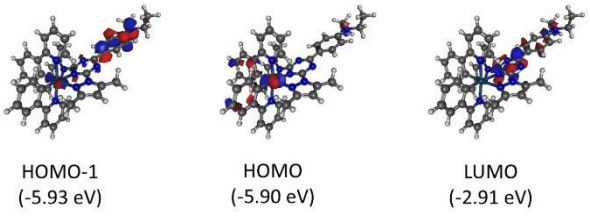

Figure 15. The HOMO-1, HOMO and LUMO orbitals of complex C2 calculated in dichloromethane.

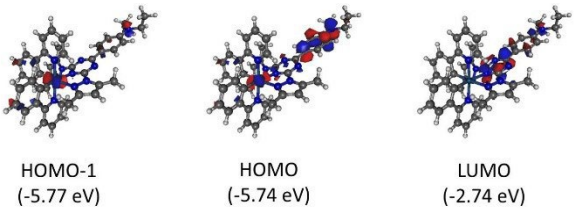

Figure 16. The HOMO-1, HOMO, and LUMO orbitals of complex C2 calculated in acetonitrile.

The proximity of the HOMO-1 and HOMO orbitals becomes even more pronounced in the calculations carried out with solvation models of dichloromethane and acetonitrile with the energy difference being only 0.03 eV. Furthermore, while in dichloromethane (Figure 15) the localization of the orbitals is the

same as in the vacuum, it is inverse in acetonitrile (Figure 16) with HOMO being localized primarily on the triazine ligand and HOMO-1 on the iridium atom and the cyclometalating ligands. These results clearly support the mixing of the intraligand and metal to ligand charge transfer (ILCT, MLCT) properties observed in the photophysical properties of **C2**. The significant contribution of the ILCT states in the photophysical properties of **C2** is likely to be the cause for the rather low intensity of emission. The weakly emissive nature of ILCT states in iridium complexes has been previously reported. The energy levels of the HOMO and LUMO orbitals are again relatively similar to that of $[Ir(ppy)_2bpy]^+$ simulated with a solvation model.[11] The presence of two closely spaced orbitals (HOMO-1, HOMO) also gives support to the observed electrochemical behavior where two oxidation waves, instead of one usually observed, are seen.

Table 2. Energies of the HOMO-1, HOMO, and LUMO orbitals for complex **C2** calculated in different environments (eV)

	HOMO-1	HOMO	LUMO
Vacuum	-7.69	-7.49	-7.69
Acetonitrile	-5.77	-5.74	-2.74
Dichloromethane	-5.93	-5.90	-2.91

Furthermore, time-dependent DFT (TDDFT) calculations were performed to model the UV-Vis spectrum of complex in dichloromethane (Figure 17). The modeled spectrum is very similar to the experimental spectrum. The major difference being the position of the band in the UV region, which has its maximum at 267 nm in the experimental spectrum while the model has the maximum of this peak at 280 nm.

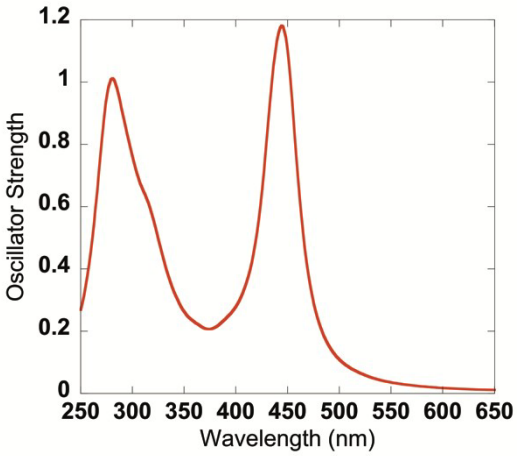

Figure 17. UV-Vis spectrum of complex **C2** modelled in dichloromethane.

Given the fact that the emission of the complex **C2**, at least in part, originates from a triplet excited state, DFT calculations for the T_1 state was carried out. The calculated distributions of the HOMO orbitals for calculations carried out in vacuum, acetonitrile, and dichloromethane can be seen in Figure 18. Furthermore, the energy differences between the T_1 and S_0 states were calculated for vacuum, acetonitrile, and dichloromethane are 2.02 eV, 1.91 eV, and 1.93 eV, respectively. These values are in relatively good agreement with the position of the observed MLCT emission band.

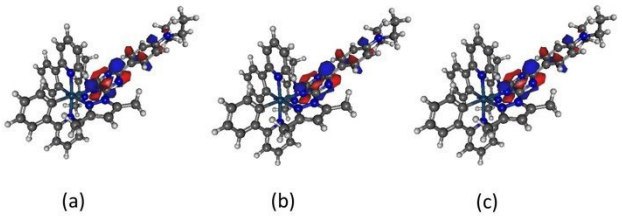

Figure 18. The HOMO orbitals of the T1 state of complex **C2** calculated in vacuum (a), acetonitrile (b), and dichloromethane (c)

Cellular Imaging

The cytotoxicity of **C2** in aqueous solution was evaluated by MTT Assay and its IC_{50} was determined to be 1.5 μM, which is extremely high compared to other cyclometalated phosphorescent Ir(III) complexes. Despite its high toxicity and weak phosphorescence, **C2** was also incubated to study if it possesses any cellular localization properties. 0.5 μM of **C2** was incubated in HeLa cells for 30 minutes and taken for confocal laser scanning microscopy imaging. Co-localization with MitoTracker Red (CMXRos) (λ_{ex} = 552 nm) confirmed the localization of **C2** in the mitochondria and the results were consistent for one-photon (λ_{ex} = 405 nm) and two-photon (λ_{ex} = 800 nm) excitation results (Figure 18). Differential interference contrast (DIC) bright field measurements were accomplished in order to determine the morphology of HeLa cells.

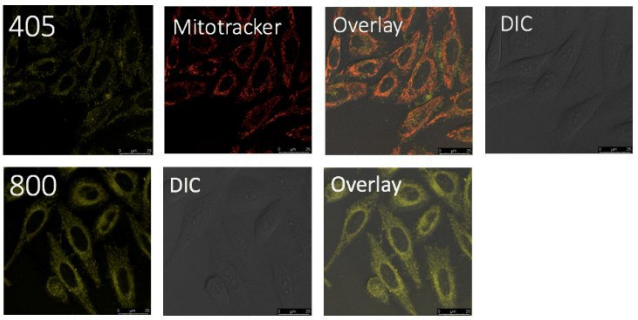

Figure 19. CLSM images of **C2**, MitoTracker and overlaid images. Emission filter: 530-580 nm (for **C2**); 600-670 nm (for Mitotracker).

Conclusions

Three N^N ligands with intraligand charge transfer character was synthesized and proposed to act as an ancillary ligand for cyclometalated iridium(III) complexes. It was found that the coordination strength of the ligands is greatly influenced by the number of electron-donating methyl substituents, and only one ligand was ultimately stable for complexation to give **C2**. Since it is only an N^N ancillary ligand, **C2** was only stable in DCM, and the ancillary ligand was found to be in a complexation-decomplexation equilibrium in MeOH over time. In ACN, however, the N^N ligand gradually decomplexed and the free ligand was regenerated. Alternatively, **C2** exhibited significantly different photophysical properties in aqueous solution compared to DCM due to the solvatochromic nature of the ancillary ligand. **C2** also demonstrated potential as a biological probe as it was found to localize at the mitochondria under two-photon excitation. Despite these results, there is still room to improve the toxicity, stability and the photophysical properties of **C2** to improve its application as a biological imaging probe.

Experimental Section

Materials and Methods

Cyanuric chloride, 4-bromo-*N*,*N*-diethylaniline, *N*,*N*-diisopropylethylamine (DIPEA), pyrazole, 2-phenylpyridine (ppy), n-butyllithium solution and spectrophotometric solvents (DCM, DMSO, ACN) were obtained from Sigma-Aldrich. *N*,*N*-diethylaniline, 3-methylpyrazole and potassium hexafluorophosphate (KPF_6) were purchased from Meryer. 3,5-dimethylpyrazole was obtained from Acros. Iridium (III) chloride hydrate ($IrCl_3$ $3H_2O$) was purchased from Precious Metals Online. Human adenocarcinoma cells (HeLa, ATCC number CCL2) were purchased from American Type Culture Collection (ATCC, VA, USA). Dulbecco's modified Eagle medium (DMEM), Phosphate-buffered saline (PBS), (3-(4,5-dimethylthiazol-2-yl)-2,5-diphenyltetrazolium bromide) or MTT solution and MitoTracker Red (CMXRos) were purchased from Thermo Fisher Scientific. 1M HEPES buffer solution and TRIS salt were purchased from Fisher.

^1H and ^{13}C NMR spectra were recorded on a Bruker Ultrashield 400 Plus NMR spectrometer (at 400 MHz and 100 MHz respectively) or a Bruker Ultrashield 600 Plus NMR spectrometer (at 600 MHz and 150 MHz respectively). The ^1H and ^{13}C NMR chemical shifts were referenced to solvent residual peaks. Mass spectra, reported as m/z, was obtained either on a Micromass Q-TOF 2 mass spectrometer or on an Agilent Technologies 6540 UHD Accurate-Mass Q-TOF LC/MS system. Cell imaging studies were performed with using Leica TCS SP8 multiphoton microscope. X-ray diffraction data was collected on a Bruker D8 Venture diffractometer. Of a total of 126233 reflections collected, 10917 were unique (R_{int} = 0.0266). The structure was solved by direct method and refined by full-matrix least squares on F2 (G.M. Sheldrick, SHELX-97, Göttingen, Germany, 1997).

All solvents used for photophysical measurements were of CHROMASOLV®Plus grade from Sigma-Aldrich and were used without further purification. Separate samples were used for 1) UV-Vis, emission and excitation scans; 2) luminescence lifetime measurements and 3) quantum yield measurements. All room temperature solution measurements were done with a quartz cuvette (Starna) of 1 cm path length. UV-Vis spectra were recorded with an HP UV-8453 spectrophotometer. Room temperature photoluminescence measurements data were obtained with Edinburgh Instruments FLSP920 spectrophotometer equipped with a Xe900 continuous xenon lamp (450 W), xenon flashlamp (60 W) and a Hamamatsu R928P cooled at -20°C. Luminescence lifetimes were measured with FLSP290 and fitted with the bundled F900 software or OriginPro.

In vitro cytotoxicity was measured by MTT Cell Proliferation Assay. Human cervix adenocarcinoma cells (HeLa) were seeded in Dulbecco's modified Eagle medium (DMEM). The MTT assay is a well-established toxicological assay to assess cell viability based on the activity of mitochondrial enzymes. 150 µL of cultured HeLa cells were added into each well of microplate and incubated with 5% CO_2 at 37°C for 24 hours. The same volume of the cell culture medium was set as the blank control. Preparation of compound was done by dissolving **C2** in DMSO (0.1% v/v). Cells were exposed to different concentrations of complex **C2** (0.313, 0.625, 1.25, 2.5, 5 and 10 µM) for, 24h. Cultured cells were removed, followed by adding 150 µL of drug. The plate was then incubated for 24 hours. Medium was removed, followed by washing with phosphate-buffered saline (PBS). 150 µL of 0.5 mg/mL (3-(4,5-dimethylthiazol-2-yl)-2,5-diphenyltetrazolium bromide) or MTT solution was added carefully in each well. After incubating 96-well plates for 4 hours, formazan crystals were observed. MTT solution was removed and 100 µL DMSO: ethanol (1:1) was added to solubilize purple crystals and incubated for 15-20 minutes. Microplate with settings of 595 nm and low shaking were used to measure the absorbance. The relative cell viability (%) of the cells exposed to complex was determined by comparing their absorption with control cells.

For cell imaging experiments, HeLa cells were seeded in Dulbecco's modified Eagle medium (DMEM) in incubator with 5% CO_2 at 37°C. 1 µL of 1 mM of complex 2 was added into the final 2 mL cell culture medium and incubated for 30min before observations. 2 µL of 1 mM MitoTracker Red (CMXRos) was added and incubated for 3 minutes in order to study specific localization of complex 2. After the completion of staining, phosphate-buffered saline (PBS) was used to replace the solution. Cell localization was studied by using Leica TCS SP8 multiphoton microscope. The excitation wavelengths used were 405nm and 800nm.

Synthesis

*Compound **1** (method 1).* A mixture of *N*,*N*-diethylaniline (13.5 g, 91 mmol) and cyanuric chloride (9.223 g, 49 mmol) was heated at 70 °C for 24 h under nitrogen. The reaction mixture was then extracted with dichloromethane and excess *N*,*N*-diethylaniline was washed away with n-hexane. The product was obtained from recrystallizing twice in acetone as a yellow/orange solid.

*Compound **1** (method 2).* *N*,*N*-diethyl-4-bromoaniline (3 g, 13 mmol) was dissolved in dry THF and the solution was kept at -78°C. n-Butyllithium (2.0 M solution in cyclohexane) (12 mL, 12.6 mmol) was added dropwise to the solution of *N*,*N*-diethyl-4-bromoaniline. A dry THF solution of cyanuric chloride (3 g, 13 mmol) was then added slowly at -78°C. The reaction was naturally warmed to room temperature after complete addition of cyanuric chloride and stirred overnight. The reaction was quenched by saturated ammonium chloride solution and THF was removed under reduced pressure. The crude was extracted with dichloromethane and water and the organic layer was dried over anhydrous magnesium sulfate and removed under reduced pressure. The crude was then chromatographed on silica with hexane/toluene (1:2) followed by recrystallization with petroleum ether to obtain the product as a yellow solid with an overall 20.2% yield. ^1H NMR ($CDCl_3$, 400 MHz): δ 1.24 (t, 6H, J=8.0 Hz), 3.47 (q, 4H, J=7.2 Hz), 6.68 (d, 1H, J=8.0 Hz), 8.32 (d, 1H, J=8.0Hz).^{13}C NMR

($CDCl_3$, 100 MHz): δ 12.43, 45.31, 111.75, 119.57, 132.47, 152.13, 170.92, 173.65.

*Compound **L1** (method A).* Pyrazole (143 mg, 2.1 mmol) was dissolved in dry THF and then dropped into a dry THF solution containing of **1** (300 mg, 1.009 mmol) and DIPEA (0.35 mL, 2.1 mmol) at room temperature. The reaction was stirred for 24 h before the solvent was removed under reduced pressure and extracted with dichloromethane. The organic layer was dried, concentrated, and chromatographed on silica with toluene/ethyl acetate (1:1), followed by purification by semi-preparative HPLC with 100% methanol to obtain a yellow oil. The product was precipitated with excess petroleum ether as a yellow solid.

*Compound **L1** (method B).* Potassium (0.389 g, 9.949 mmol) was added to a stirred dry THF solution of pyrazole (0.975 g, 14.321 mmol) under N_2 at room temperature. The reaction mixture was refluxed until all potassium disappeared and cooled to 4°C. **1** (1.106 g, 3.721 mmol) was then added and stirred for 1 h before refluxing for overnight. The THF was removed under reduced pressure and the crude was extracted with dichloromethane. The crude was then chromatographed on silica with dichloromethane/ethyl acetate (10:1) and then purified by preparative HPLC with 100% methanol to give a yellow oil. The product was precipitated with excess petroleum ether as a yellow solid with an overall yield of 50.9%. ^{1}H NMR ($CDCl_3$, 400 MHz): δ 1.23 (t, 6H, J=8.0 Hz), 3.45 (q, 4H, J=7.2 Hz), 6.54 (q, 1H, J=1.5 Hz), 6.71 (d, 1H, J=8.8 Hz), 7.92 (d, 1H, J=0.8 Hz), 8.52 (d, 1H, J=12.0 Hz), 8.79 (d,1H, J=2.4 Hz).^{13}CNMR ($CDCl_3$, 100 MHz): δ 12.59, 44.67, 109.39, 110.69, 120.25, 130.13, 131.98, 14492, 152.14, 162.60, 174.20. m/z (ESI-MS), 361.1882[M+1]$^+$

*Compound **L2**.* The synthesis is the same as **L1**. The crude was purified by column chromatography with chloroform/ethanol (10:1) to yield yellowish needle-like crystals as product with an overall 32.3% yield. ^{1}H NMR ($CDCl_3$, 400 MHz): δ 1.24 (t, 6H, J=8.0Hz), 2.35 (s, 3H), 2.86 (s, 3H), 3.47 (q, 4H, J=7.2 Hz), 6.08 (s, 1H), 6.74 (d, 1H, J=8.0 Hz), 8.38 (d, 1H, J=8.0 Hz). ^{13}C NMR ($CDCl_3$ 100 MHz): δ 12.59, 13.82, 16.22, 44.67, 110.79, 111.40, 121.17, 131.41, 144.08, 151.64, 152.56, 163.88, 173.19. m/z (ESI-MS), 417.251[M+1]$^+$

*Compound **L3**.* The synthesis and purification is the same as **L1**. The product was obtained as a yellow solid with an overall yield of 36.1%. ^{1}H NMR ($CDCl_3$, 400 MHz): δ 1.040 (t, 6H, J=7.2 Hz), 1.884 (s, 3H), 3.25 (q, 4H, J=6.8 Hz), 6.182 (d, 1H, J=2.0 Hz), 6.527 (d, 1H, J=8.8 Hz),8.325 (d, 1H, J=8.8 Hz), 8.514 (d, 1H, J=2. 4Hz). ^{13}C NMR ($CDCl_3$, 100 MHz): δ 12.59, 14.23, 44.63, 109.33, 110.59, 120.50, 130.77, 131.81, 151.89, 154.78, 162.25, 173.85. m/z (ESI-MS), 389.220[M+1]$^+$

*Compound **2**.*[5] A mixture of 2-phenylpyridine (1.123 g, 7.234 mmol), $IrCl_3 \cdot 3H_2O$ (1.01 g, 2.864 mmol) in 60 mL of degassed 2-ethoxyethanol/water (3:1) was refluxed under N_2 at 130°C for 20 h. The reaction mixture was then cooled to room temperature and washed with centrifugation with water, ethanol, and acetone. The product was collected as yellow solid with a 79.94% yield. ^{1}H NMR ($CDCl_3$, 400 MHz): δ 5.935 (d, 1H, J=7.2 Hz), 6.559 (d, 1H, J=6.4 Hz), 6.723-6.788 (m, 2H), 7.491 (d, 1H, J=6.4 Hz), 7.732 (t, 1H, J=7.2 Hz), 7.877 (d, 1H, J=8.0 Hz), 9.247 (d, 1H, J=5.6 Hz) ^{13}C NMR ($CDCl_3$, 100 MHz): δ 118.37, 121.31, 122.09, 123.64, 129.09, 130.57, 136.14, 143.70, 145.32, 151.70, 168.56.

*Compound **C1** (method A).* **2** (29.8 mg, 0.028 mmol) and **L1** (25.0 mg, 0.069 mmol) were dissolved in 5 mL of dichloromethane/methanol (2:1) and refluxed overnight under nitrogen. The reaction mixture was cooled to room temperature and excess KPF_6 was added. The reaction mixture was then stirred overnight, filtered, and the solvent was removed in vacuo. The crude was chromatographed on silica with dichloromethane/methanol to yield a yellow solid (14.9 mg). ^{1}H NMR ($CDCl_3$, 400 MHz): δ 1.243 (t, 6H, J=7.1 Hz), 3.482 (q, 4H, J=7.1 Hz), 3.586 (s, 3H), 6.212 (d, 1H, J=7.5 Hz), 6.281 (d, 1H, J=7.2 Hz), 6.714 (s, 1H), 6.737 (s, 1H), 6.823 (m, 1H), 6.860 (t, 2H, J=7.6 Hz), 6.945 (t, 1H, J=8.4 Hz), 7.025 (t, 1H, J=6.8 Hz), 7.137 (t, 1H, J=6.0 Hz), 7.206 (1H, d, J=6.0 Hz), 7.231 (1H, s), 7.568 (1H, d, J=6.0 Hz), 7.637 (2H, t, J=7.8 Hz), 7.824 (2H, m), 7.924 (2H, t, J=6.9 Hz), 8.174 (1H, d, J=5.3 Hz), 8.403 (2H, d, J=9.0 Hz), 8.961 (1H, d, J=3.0 Hz) ^{13}C NMR ($CDCl_3$, 400 MHz): δ 12.66, 29.83, 56.39, 112.46, 118.34, 119.01, 119.42, 119.59, 121.38, 121.770, 122.775, 123.320, 123.697, 124.00, 124.51, 129.83, 130.48, 131.55, 131.83, 132.32, 133.25, 133.50, 138.35, 143.48, 143.77, 144.14, 145.24, 148.53, 149.20, 149.32, 150.27, 167.55, 168.73 (ESI-MS), 825.2632[M]$^+$

*Compound **C1** (method B).* **2** (67.1 mg, 0.063 mmol) and **L1** (44.8 mg, 0.124 mmol) were dissolved in 12 mL of dichloromethane/acetonitrile (2:1) and refluxed overnight under nitrogen. The reaction mixture was cooled to room temperature and excess KPF_6 was added. The reaction mixture was then stirred overnight and filtered. The crude was extracted with dichloromethane.

*Compound **C2** (method A).*[12] **2** (25.7 mg, 0.024 mmol) and **L2** (20 mg, 0.048 mmol) were dissolved in 10 mL of dichloromethane:methanol (2:1) and refluxed at 90°C overnight under nitrogen. The reaction mixture was cooled and the solvent were removed under reduced pressure. The solids were re-dissolved in 10 mL of methanol and excess KPF_6 was added and stirred for 10min at room temperature until all the precipitate out completely. The precipitate was isolated by centrifugation (4000 rpm, 5 min) and further washed twice with methanol with centrifugation. The complex **C2** was dried under high vacuum for a prolonged period to yield 25.0 mg (57.0%) of an orange solid. ^{1}H NMR (MeOD, 400 MHz): δ 1.234 (t, 6H, J=14 Hz), 1.549 (s, 3H), 1.938 (s, 3H), 2.038 (s, 3H), 3.086 (s, 3H), 3.554 (q, 4H, J=20.8 Hz), 5.866 (d, 1H, J=6.8 Hz), 6.023 (d, 1H, J=8.0 Hz), 6.472 (s, 1H), 6.529 (t, 1H, J=14.8 Hz), 6.664 (q, 2H, J=22.4 Hz), 6.832 (d, 2H, J=9.2 Hz) 6.912 (t, 1H, J=14.4 Hz), 7.140 (t, 1H, J=14.4 Hz), 7.315 (t, 1H, J=12.8 Hz), 7.485 (d, 1H, J=8.4 Hz), 7.696 (d, 1H, J=5.2 Hz), 7.764(d, 1H, J=7.6 Hz), 7.846 (t, 1H, J=16.4 Hz), 8.010(d, 2H, J=8.0 Hz), 8.136 (d, 2H, J=8.0 Hz), 8.229 (d, 2H, J=8.4 Hz), 9.429 (s, 1H). ^{13}C NMR ($CDCl_3$, 100 MHz): δ 12.06, 12.54, 12.82, 13.74, 15.79,29.70, 45.03,110.36, 111.51. 114.93, 118.27, 118.93, 121.62, 121.79, 122.33, 122.37, 123.75, 124.50, 128.18, 130.00, 131.36, 132.64, 133.12, 138.09, 138.72, 141.52, 142.38, 143.06, 143.50, 146.99, 148.10, 148.43, 152.16, 153.50, 154.50, 158.10, 162.81, 163.56, 166.99, 167.88, 170.79. m/z (ESI-MS), 917.3343[M]$^+$

*Compound **C2** (method B).* **2** (108.3 mg, 0.101 mmol) and **L2** (107.5 mg, 0.258 mmol) were dissolved in acetonitrile and refluxed overnight under nitrogen. Excess KPF_6 was added to the cooled reaction mixture and was stirred at room temperature overnight. The reaction mixture was filtered, and the filtrate was extracted with dichloromethane. The crude was chromatographed on silica with dichloromethane/acetone (10:1) and the product was obtained as an orange solid with an overall yield of 6.1%.

*Compound **C3** (method A).* **2** (60.0 mg, 0.060 mmol) and **L3** (50.0 mg, 0.13 mmol) were dissolved in 10 mL of dichloromethane/methanol (2:1) and refluxed overnight under nitrogen. The reaction mixture was cooled to room temperature and excess KPF_6 was added. The reaction mixture was then stirred overnight, filtered, and the solvent was removed in vacuo. The crude was chromatographed on silica with dichloromethane/methanol to yield a yellow solid (27.6 mg). (ESI-MS), 839.2811[M]$^+$

*Compound **C3** (method B).* **2** (34.307 mg, 0.032 mmol) and **L3** (24.2 mg, 0.0623 mmol) were dissolved in 6 mL of dichloromethane/acetonitrile (2:1) and refluxed overnight under nitrogen. The reaction mixture was cooled to room temperature and excess KPF_6 was added. The reaction mixture was

then stirred overnight and filtered. The crude was extracted with dichloromethane.

Electrochemistry

n-Tetrabutylammonium hexafluorophosphate ($TBAPF_6$) and anhydrous acetonitrile were supplied by Sigma–Aldrich. The indifferent electrolyte $TBAPF_6$ was dried under vacuum. Acetonitrile was dried over activated molecular sieves. Electrochemical measurements were performed using AUTOLAB instrument PGSTAT 302N (Metrohm). An electrochemical data from cyclic voltammetry were analyzed using AUTOLAB software. A three-electrode electrochemical cell was used. The reference electrode (RE), Ag|AgCl|1 M LiCl, was separated from the test solution by a salt bridge. The working electrode (WE) was Pt disk (d = 2 mm). The auxiliary electrode was platinum net. The scan rate for the cyclic voltammetry was in the range 16–512 mV s^{-1}. Oxygen was removed from the solution by passing a stream of argon saturated with vapors of the solvent.

Crystal Structure- CCDC-1561475

Crystals of complex **C2** suitable for X-ray diffraction were obtained by diffusion of hexane into its solution in acetone. Complex **C2** crystalizes in the triclinic unit cell with a space group *P-1*. Although both *P1* and *P-1* were suggested as reasonable space group for the structure, refinement of the structure failed to converge towards the final stages; whereas the low *R*-values {*R1* = 0.0180 [I > 2σI] and *wR2* = 0.0434 (all data)} confirms that *P-1* is indeed the correct space group. The asymmetric unit contains the complex with its hexafluorophosphate counter ion and a molecule of acetone (Figure 2). The Ir(III) center adopts a distorted octahedral geometry with a typical trans arrangement of the nitrogen atoms from the cyclometalating 2-phenylpyridine ligands. The structural parameters within the coordination sphere of the iridium atom are analogous to other biscyclometalated iridium complexes.[4d-e] Thus the Ir-N bond distances for the N^N ligand, 2.198 Å for the Ir1-N4 bond and 2.148 Å for the Ir1-N6 bond, are longer than the Ir-N bond distances in the phenyl pyridine ligands (~2.05 Å). This has been previously explained by the strong trans influence of the carbon atom of the 2-phenylpyridine ligand. Furthermore, the bite angle of the N^N ligand is smaller, 74.07(6) for the N4-Ir1-N6 angle, than the bite angles of the phenyl pyridine ligands (~80.2). Finally, the structure shows that the non-coordinated pyrazole ring is not coplanar with the rest of the ligand with the torsion angle N8-N7-C13-N4 being -57.8(2) while the coordinated pyrazole ring is nearly coplanar with the triazine one with N6-N5-C12-N4 torsion angle of -7.8(2). Crystal data for **C2**: C_{48} H_{50} F_6 Ir N_{10} O_1 P_1, M_r = 1120.15, Triclinic, space group *P-1*, Z = 2, a = 9.2915(5) Å, b = 10.8140(6) Å, c = 24.7923(14) Å, α = 86.7856(14)°, β = 85.7856(14)°, γ = 73.1408(13)°, V = 2375.5(2) $Å^3$, $\mu(Mo_{K\alpha})$ = 2.916 mm^{-1}, ρ_{calc} = 1.566 mgm^{-3}, T = 296(2) K.

DFT Calculations

Calculations were carried out with the Gaussian09 software package[13] at the DFT level, using the hybrid functional B3LYP and the double-zeta basis set LANL2DZ. The calculations were carried out for a vacuum environment as well as acetonitrile (ε = 35.688) and dichloromethane (ε = 8.93) using the polarizable continuum model. The molecular orbitals were visualized using the Gabeit program package.[13]

Acknowledgements

GLL acknowledges The Hong Kong Polytechnic University (4BCC8) and the Research Grants Council, University Grants Committee Hong Kong (PolyU 253002/14P). The University Research Facility in Life Sciences (ULS), the University Research Facility for Chemical and Environmental Analysis (UCEA) for an Area of Excellence Grant (1-ZVGG) and the Natural Science Foundation of China -NSFC (21401158)

The National e-Science Infrastructure Consortium (NECTEC) is acknowledged for providing computing resources that have contributed to the research results reported within this paper. The authors also acknowledge financial support from the Thailand Research Fund (RSA6080041).

MG acknowledges the support from the Slovak Research and Development Agency under project number APVV-17-0149.

Keywords: iridium • intra-ligand charge transfer • phosphorescence • mitochondria

[1] a) Y. You, S. Y. Park, *Dalton Trans*. **2009**, 1267-1282; b) Y. You, W. Nam, *Chem. Soc. Rev*. **2012**, *41*, 7061-7084; c) Y. You, *Curr. Opin. Chem. Biol.* **2013**, *17*, 699-707; d) M. P. Coogan, V. Fernandez-Moreira, *Chem. Commun.* **2014**, *50*, 384-399; e) K. K.-W. Lo, *Acc. Chem. Res*. **2015**, *48*, 2985-2995.

[2] Q, Zhao, M. Yu, L. Shi, S. Liu, C. Li, M. Shi, Z. Zhou, C. Huang, F. Li, *Organometallics* **2010**, *29*, 1085-1091.

[3] Y. You, J. Seo, S. Kim, K. Kim, T. Ahn, D. Kim, S. Park, *Inorg. Chem.* **2008**, *47*, 1476-1487.

[4] a) M. G. Colombo, H. U. Güdel, *Inorg. Chem.* **1993**, *32*, 3081-3087; b) L. Jian, P. I. Djurovich, B. D. Alleyne, M. Yousufuddin, N. N. Ho, J. C. Thomas, J. C. Peters, R. Bau, M. E. Thompson, *Inorg. Chem.* **2005**, *44*, 1713-1727; c) E. Orselli, G. Kottas, A. Konradsson, P. Coppo, R. Fröhlich, L, De Cola, A. van Dijken, M. Büchel, H. Börner, *Inorg. Chem.* **2007**, *46*, 11082-11093; d) J. B. Waern, C. Desmarets, L.-M. Chamoreau, H. Amouri, A. Barbieri, C. Sabatine, B. Ventura, F. Barigelletti, *Inorg. Chem.* **2008**, *47*, 3340-3348; e) S. Ladouceur, F. Zysman-Colman, *Eur. J. Inorg. Chem.* **2013**, *17*, 2985-3007; f D. N. Chirdon, W. J. Transue, H. N. Kagalwala, A. Kaur, A. B. Maurer, T. Pintauer, S. Bernhard, *Inorg. Chem.* **2014**, *53*, 1487-1499.

[5] J. Jesu Raj, M. Quintanilla, F. Vetrone, *J. Mater. Chem. B* **2016**, *4*, 3113-3120.

[6] a) W.-S. Lo, J. Zhang, W.-T. Wong, G.-L. Law, *Inorg. Chem.* **2015**, *54*, 3725-3727; b) W.-S. Lo, W.-T. Wong, G.-L. Law, *RSC Adv.* **2016**, *6*, 74100-74109.

[7] M. Albota, D. Beljonne, J. L. Bredas, J. E. Ehrlich, J. Y. Fu, A. A. Heikal, S. E. Hess, T. Kogej, M. D. Levin, S. R. Marder, D. McCord-Maughon, J. W. Perry, H. Rockel, M. Rumi, C. Subramaniam, W. W. Webb, X. L. Wu, C. Xu, *Science* **1998**, *281*, 1653– 1656.

[8] a) K. Svoboda, R. Yasuda, *Neuron* **2006**, *50*, 823-839; b) H. Huang, L. Yang, P. Zhang, K. Qiu, J. Huang, Y. Chen, J. Diao, J. Liu, L. Ji, J. Long, H. Chao, *Biomaterials* **2016**, *83*, 321-331.

[9] I. B. Berlman. Handbook of Fluorescence Spectra of Aromatic Molecules, Academic Press, New York (1971).

[10] R. D. Costa, E. Ortí, H. J. Bolink, S. Graber, S. Schaffner, M. Neuburger, C. E. Housecroft, E. C. Constable, *Adv. Funct. Mater.* **2009**, *19*, 3456-3463.

[11] E. C. Constable, M. Neuburger, P. Rösel, B. E. Schneider, J. A. Zampese, C. E. Housecroft, F. Monti, N. Armaroli, R. D. Costa, E. Ortí, *Inorg. Chem.* **2013**, *52*, 885-897.

[12] S. Soman, G. S. Bindra, A. Paul, R. Groarke, J. C. Manton, F. M. Connaughton, M. Schulz, D. Dini, C. Long, M. T. Pryce, J. G. Vos, *Dalton Trans.* **2012**, *41*, 12678-12680.

[13] Gaussian 09, Revision **D.01**, M. J. Frisch, G. W. Trucks, H. B. Schlegel, G. E. Scuseria, M. A. Robb, J. R. Cheeseman, G. Scalmani, V. Barone, B. Mennucci, G. A. Petersson, H. Nakatsuji, M. Caricato, X. Li, H. P. Hratchian, A. F. Izmaylov, J. Bloino, G. Zheng, J. L. Sonnenberg, M. Hada, M. Ehara, K. Toyota, R. Fukuda, J. Hasegawa, M. Ishida, T. Nakajima, Y. Honda, O. Kitao, H. Nakai, T. Vreven, J. A. Montgomery, Jr., J. E. Peralta, F. Ogliaro, M. Bearpark, J. J. Heyd, E. Brothers, K. N. Kudin, V. N. Staroverov, R. Kobayashi, J. Normand, K. Raghavachari, A. Rendell, J. C. Burant, S. S. Iyengar, J. Tomasi, M. Cossi, N. Rega, J. M. Millam, M. Klene, J. E. Knox, J. B. Cross, V. Bakken, C. Adamo, J. Jaramillo, R. Gomperts, R. E. Stratmann, O. Yazyev, A. J. Austin, R. Cammi, C. Pomelli, J. W. Ochterski, R. L. Martin, K. Morokuma, V. G. Zakrzewski, G. A. Voth, P. Salvador, J. J. Dannenberg, S. Dapprich, A. D. Daniels, Ö. Farkas, J. B. Foresman, J. V. Ortiz, J. Cioslowski, and D. J. Fox, Gaussian, Inc., Wallingford CT, 2009.

[13] A. R. Allouche, *J. Compt. Chem.* **2011**, *32*, 174-182.

FULL PAPER

In this work, the synthesis, stability studies and photophysical properties of a bis-cyclometalated iridium(III) complex with a push-pull ancillary ligand are presented. The complex was found to localize in mitochondria and could be excited by a two-photon excitation process under a confocal laser scanning microscope.

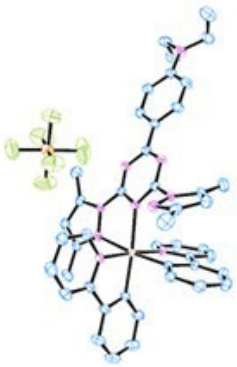

Iridium phosphorescence

Poonnapa Zheng, Pawittra Chaibuth, Wai-Sum Lo, Weiweij Jin, Xinyang Sun, Sureemas Meksawangwong, Wikorn Punyain, Miroslav Gál, Yanjuan Gu, Wesley Ting Kwok Chan, Filip Kielar, Ga-Lai Law**

Page No. – Page No.

Study of two photon iridium complex containing dipyrazolyltriazine as cellular imaging dyes